Research Square

Preprints are preliminary reports that have not undergone peer review.
They should not be considered conclusive, used to inform clinical practice,
or referenced by the media as validated information.

Integrated network pharmacology, molecular docking, molecular dynamics simulation, and in vitro validation suggest that diosmin attenuates acute-cystitis-related inflammatory injury in SV-HUC-1 human urothelial cells

Tianhao Zhang

zhangaaa88@163.com

Department of Urology,QIAN WEI HOSPITAL OF JILIN PROVINCE

Nuerzhati Yishamudong

Jilin University School of Nursing

Chao Zhang

Department of Urology,QIAN WEI HOSPITAL OF JILIN PROVINCE

Dongqi Zhang

Department of Urology,QIAN WEI HOSPITAL OF JILIN PROVINCE

Tinghe Yan

Jilin University Physical Education College

Research Article

Keywords: Diosmin, acute cystitis, network pharmacology, MMP-9

Posted Date: September 29th, 2026

DOI: https://doi.org/10.21203/rs.3.rs-10990311/v1

License: This work is licensed under a Creative Commons Attribution 4.0 International License.
Read Full License

Additional Declarations:
No competing interests reported.

Table 1 is available in the Supplementary Files section.

Integrated network pharmacology, molecular docking, molecular dynamics simulation, and in vitro validation suggest that diosmin attenuates acute-cystitis-related inflammatory injury in SV-HUC-1 human urothelial cells

Tianhao Zhang[a, †, *], Nuerzhati Yishamudong[b, †], Chao Zhang[a], Dongqi Zhang[a], , Tinghe Yan[c]

[a] Department of Urology,QIAN WEI HOSPITAL OF JILIN PROVINCE,Changchun, Jilin Province, 130032, China.

[b] School of Nursing, Jilin University, Changchun, Jilin Province, 130021, China.

[c] College of Physical education , Jilin University, Changchun, Jilin Province, 130021, China.

[†]Tianhao Zhang and Nuerzhati Yishamudong contributed equally to this work and share the first authorship.

* Address correspondence requests to Tianhao Zhang, QIAN WEI HOSPITAL OF JILIN PROVINCE, Changchun 130021, Jilin, China. Tel: +86-13756534604, E-mail:zhangaaa88@163.com

Statements and Declarations

Ethics approval and consent to participate

Not applicable. (This study did not involve human participants, animal experiments, or clinical trials that require ethical approval.)

Consent for publication

Not applicable. (This manuscript does not contain any individual person’s data in any form.)

Availability of data and material

The data supporting the findings of this study are available from the corresponding author upon reasonable request. The public transcriptomic datasets analyzed in this study are available in the NCBI Gene Expression Omnibus (GEO) under accession numbers GSE33210 and GSE26509. All other data generated or analyzed during this study are included in this published article and its supplementary information files.

Competing interests

The authors declare that they have no competing interests.

Funding

This research received no specific grant from any funding agency in the public, commercial, or not-for-profit sectors.

Acknowledgements

Not applicable.

Abstract

Acute cystitis is a common lower urinary tract infection, most frequently caused by uropathogenic Escherichia coli, and excessive host inflammatory and nitrosative responses can impair urothelial homeostasis and cause mucosal injury. Diosmin, a citrus-derived flavonoid glycoside, has anti-inflammatory and antioxidant activities, but its effects on acute-cystitis-related urothelial injury and underlying molecular targets remain unclear. This study investigated the protective effects and mechanisms of diosmin using network pharmacology, molecular docking, molecular dynamics simulation, and in vitro validation in SV-HUC-1 human urothelial cells. Candidate diosmin targets were predicted using SwissTargetPrediction and SEA, and acute-cystitis-related genes were collected from GEO datasets (GSE33210, GSE26509), GeneCards, GenCLiP, and OMIM. Eleven overlapping targets were identified, with TNF and MMP-9 ranking highest by network degree. Molecular docking yielded binding energies of -9.3 kcal/mol for diosmin-MMP-9 and -8.0 kcal/mol for diosmin-TNF, and a 100-ns simulation supported a stable diosmin-MMP-9 complex. GO enrichment implicated inflammatory responses, proliferation, migration, and adhesion, while KEGG analysis highlighted TNF and IL-17 signaling. In LPS-stimulated SV-HUC-1 cells, 80 μM diosmin did not significantly reduce viability and improved colony formation, reduced NO accumulation, and attenuated MMP-9 and TNF-α protein increases. Thus, diosmin attenuated LPS-induced inflammatory injury in urothelial cells, associated with reduced MMP-9 and TNF-α expression. These hypothesis-generating findings require confirmation in infection-based animal models and target-specific genetic experiments.

Keywords: Diosmin; acute cystitis; network pharmacology; MMP-9.

1. Introduction

Acute cystitis is among the most common bacterial infections of the lower urinary tract, and uropathogenic Escherichia coli (UPEC) is the predominant pathogen in uncomplicated disease [1-4]. Antimicrobial therapy remains the mainstay of treatment; however, the global burden of antimicrobial resistance underscores the need for complementary strategies that can limit tissue injury without increasing antibacterial selection pressure [4, 5]. At the urothelial surface, UPEC can adhere to and invade bladder epithelial cells, form intracellular bacterial communities, persist within the urinary tract, and provoke host responses that shape both bacterial clearance and recurrent disease[6-10] . These host-pathogen interactions can disrupt urothelial homeostasis and repair, providing a biological rationale for investigating agents that modulate excessive inflammatory injury while preserving epithelial recovery.

Diosmin is a naturally occurring flavone glycoside found predominantly in citrus species. Pharmacological reviews and experimental studies have described anti-inflammatory, antioxidant, and cytoprotective properties of diosmin across several tissue and cell-injury models [11-19]. In LPS-stimulated macrophages

and neuronal cells, diosmin has been reported to reduce pro-inflammatory mediator production and TNF-α-associated responses[15, 16], while studies in other epithelial or connective-tissue systems suggest broader effects on oxidative stress and matrix-remodeling pathways [17-19]. Nevertheless, direct evidence for diosmin in acute cystitis is limited, and its candidate molecular targets in inflamed human urothelial cells have not been systematically characterized.

Network pharmacology provides a framework for integrating compound-target and disease-gene information to generate testable hypotheses about multi-target natural products [20]. When combined with molecular docking, molecular dynamics simulation, and experimental validation, this approach can prioritize candidate interactions while recognizing that in silico binding predictions alone do not establish target engagement or causality. Accordingly, the present study integrated target mining, protein-protein interaction (PPI) analysis, functional enrichment, molecular docking, molecular dynamics simulation, and cellular experiments to investigate the potential actions of diosmin in an acute-cystitis-related inflammatory injury model.

Specifically, we sought to (i) identify overlapping diosmin and acute-cystitis-related targets; (ii) prioritize hub proteins and enriched biological pathways; (iii) evaluate the structural plausibility and dynamic stability of diosmin binding to candidate hub proteins; and (iv) test whether diosmin modifies LPS-induced changes in SV-HUC-1 cell viability, colony-forming capacity, NO production, and MMP-9/TNF-α protein expression. This integrated workflow was intended to generate a mechanistic hypothesis suitable for subsequent validation in infection-based animal models and target-specific rescue experiments.

2. Materials and methods

2.1 Reagents and antibodies

Diosmin (purity ≥98%, CAS 520-27-4) was obtained from Shanghai Yuanye Biotechnology Co., Ltd. (Shanghai, China). Lipopolysaccharide (LPS; Escherichia coli O111:B4) was purchased from Sigma-Aldrich (St. Louis, MO, USA), and dimethyl sulfoxide (DMSO) was obtained from Solarbio Science & Technology Co., Ltd. (Beijing, China).

Primary antibodies against MMP-9 (Cat. No. AF5228) and TNF-α (Cat. No. AF7014), together with horseradish-peroxidase-conjugated goat anti-rabbit IgG secondary antibody (Cat. No. S0001), were obtained from Affinity Biosciences (Changzhou, China). anti-IL-17 (Cat. No. 13082-1-AP) was obtained Proteintech.GAPDH antibody (Cat. No. F2511) was obtained from Selleck. The BCA protein-quantification kit (Cat. No. P0010S) and enhanced chemiluminescence (ECL) kit (Cat. No. P0018M) were purchased from Beyotime Biotechnology (Shanghai, China).

Cell Counting Kit-8 (CCK-8; Cat. No. G4103) was supplied by Servicebio (Wuhan, China). The nitric oxide assay kit (Cat. No. A012-1-2) was purchased

from Nanjing Jiancheng Bioengineering Institute (Nanjing, China).

2.3 Network-pharmacology target identification

Potential protein targets of diosmin were predicted using SwissTargetPrediction [21] and the Similarity Ensemble Approach (SEA) [22]. Acute-cystitis-related genes were collected from GeneCards [23], GenCLiP [24], and OMIM [25]. In parallel, the GEO datasets GSE33210 and GSE26509 were retrieved from the NCBI Gene Expression Omnibus [26]. Differential-expression analysis was performed using GEO2R with thresholds of $|\log_2 \text{fold change}| > 1$ and adjusted $P < 0.05$. Gene identifiers were standardized and duplicate entries were removed before intersection of the diosmin-target and acute-cystitis-related gene sets. A Venn diagram was used to visualize shared candidate targets.

2.4 PPI network construction and hub-gene filtering

Shared candidate targets were submitted to STRING (version 11.5) to construct a PPI network with the minimum interaction confidence score set to >0.7 [27]. The interaction table was imported into Cytoscape 3.9.1 for network visualization and topological analysis [28]. Node degree was calculated for each target, and the two targets with the highest degree values were prioritized as hub genes for subsequent structural and experimental analyses.

2.7 GO and KEGG enrichment analysis

Functional enrichment was performed in R (version 4.2.1) using clusterProfiler [29, 30]. Gene Ontology (GO) terms[31]and Kyoto Encyclopedia of Genes and Genomes (KEGG) pathways[32] were evaluated, with $P < 0.05$ used as the enrichment threshold. Bar plots and bubble plots were generated with ggplot2.

2.5 Molecular docking

Crystal structures of MMP-9 (PDB ID: 1L6J) and TNF (PDB ID: 1TNF) were retrieved from the RCSB Protein Data Bank [33], and the two-dimensional structure of diosmin (PubChem CID 5281608) was obtained from PubChem [34]. Proteins and ligand structures were prepared using AutoDockTools 1.5.7 by removing crystallographic water molecules and original ligands where appropriate and adding polar hydrogens. Docking grids were centered on the relevant binding pockets. AutoDock Vina was used for docking [35], and the lowest-energy poses were recorded and visualized in PyMOL 2.5.

2.6 Molecular dynamics simulation

The top-ranked diosmin-MMP-9 docking complex was subjected to a 100-ns molecular dynamics simulation using GROMACS 2022.3[36]. The CHARMM36 force field was used for the protein [37], and the system was solvated with the TIP3P water model [38]. Sodium and chloride ions were added

to neutralize the system. Energy minimization, NVT equilibration, NPT equilibration, and the production simulation were performed sequentially. Trajectory analyses included root-mean-square deviation (RMSD), root-mean-square fluctuation (RMSF), radius of gyration (Rg), solvent-accessible surface area (SASA), and hydrogen-bond analysis. MM-PBSA calculations were used to estimate binding free-energy contributions and residue-wise energetic contributions using a GROMACS-compatible workflow[39].

2.2 Cell culture

The human urothelial cell line SV-HUC-1 was obtained from the American Type Culture Collection (ATCC, Manassas, VA, USA). Cells were cultured in DMEM/F12 medium supplemented with 10% fetal bovine serum (Gibco, Thermo Fisher Scientific, Waltham, MA, USA), 100 U/mL penicillin, and 100 μg/mL streptomycin, and maintained at 37 °C in a humidified atmosphere containing 5% CO_2.

2.8 CCK-8 cell-viability assay

SV-HUC-1 cells were seeded in 96-well plates at 5×10^3 cells per well and allowed to adhere overnight. Cells were then exposed for 24 h to graded concentrations of LPS (0, 0.25, 0.5, 1.0, and 2.0 μg/mL) or diosmin (0-90 μM). CCK-8 reagent (10 μL/well) was added and incubated for 2 h at 37 °C, and absorbance at 450 nm was measured using a Tecan Spark microplate reader (Männedorf, Switzerland). The CCK-8 assay is based on reduction of a water-soluble tetrazolium salt by metabolically active cells [40].

2.9 Colony-formation assay

SV-HUC-1 cells were seeded in six-well plates at 800 cells per well. The experimental groups were: control; LPS injury (1 μg/mL LPS); and diosmin intervention (80 μM diosmin pretreatment for 1 h followed by co-incubation with 1 μg/mL LPS). Medium was refreshed every 3 days. After 14 days, colonies were fixed with 4% paraformaldehyde and stained with crystal violet. Colony-formation assays were performed according to established clonogenic-assay principles [41].

2.10 Measurement of NO concentration

Cell-culture supernatants were collected after 24 h of the indicated treatments. NO-related products were quantified using a nitrate-reductase-based commercial kit according to the manufacturer's instructions. Absorbance was read at 550 nm and concentrations were calculated from the supplied standard curve. Quantification of nitrite/nitrate is a widely used surrogate approach for assessing NO production in biological samples [42].

2.11 Western blot analysis

Total cellular protein was extracted in RIPA lysis buffer supplemented with protease inhibitors, and protein concentration was determined by BCA assay. Equal amounts of protein were separated by 10% SDS-PAGE and transferred to PVDF membranes. Membranes were blocked with 5% skim milk for 1.5 h at room temperature and incubated overnight at 4 °C with primary antibodies against MMP-9 (1:1000), IL-17 (1:1000), TNF-α (1:1000), and GAPDH (1:1000). After TBST washing, membranes were incubated with secondary antibody (1:5000) for 1 h at room temperature. Bands were visualized using ECL, and GAPDH served as the loading control. The transfer procedure followed the general principles of western blotting.

2.12 Statistical analysis

Quantitative data are presented as mean ± standard deviation (SD). Statistical analyses and graphing were performed using GraphPad Prism 10 (GraphPad Software, San Diego, CA, USA). One-way analysis of variance (ANOVA) followed by Tukey's post hoc multiple-comparison test was used for comparisons among multiple groups. A two-sided $P < 0.05$ was considered statistically significant. Cellular experiments were independently repeated three times ($n = 3$)[43].

3. Results

3.1 Identification of overlapping therapeutic targets between diosmin and acute-cystitis-related genes

Differential-expression analysis of GSE33210 and GSE26509 identified genes associated with the acute-cystitis-related transcriptomic phenotype (Supplementary Figure 1). Disease-associated genes were further supplemented using GeneCards, GenCLiP, and OMIM, while putative diosmin targets were obtained from SwissTargetPrediction and SEA. After identifier harmonization and removal of duplicates, intersection analysis yielded 11 shared genes (Figure 1), which were carried forward as candidate diosmin targets relevant to acute cystitis.

3.2 PPI network construction and hub-gene screening

The 11 overlapping genes were submitted to STRING to generate a PPI network and then imported into Cytoscape for topological analysis. TNF and MMP-9 showed the highest degree values among the candidate nodes and were therefore prioritized as hub targets for subsequent docking, molecular dynamics, and cellular validation (Figure 2; Table 1). These rankings indicate network centrality within the analyzed target set rather than proof of functional indispensability.

3.3 GO functional enrichment and KEGG pathway enrichment

GO enrichment identified biological-process terms related to inflammatory responses, regulation of cell proliferation, cell migration, and cell adhesion. Cellular-component terms were enriched in extracellular and membrane-associated categories, whereas molecular-function terms included cytokine-related and protease-related functions (Figure 3). KEGG analysis highlighted the TNF and IL-17 signaling pathways among the enriched pathways (Figure 4). These findings were used to guide the selection of phenotypic and molecular readouts for subsequent cellular experiments.

3.4 Molecular docking and 100-ns molecular dynamics simulation

Molecular docking was performed to compare the predicted binding of diosmin to the two hub proteins. The docking energy was -8.0 kcal/mol for the diosmin-TNF complex and -9.3 kcal/mol for the diosmin-MMP-9 complex (Figure 5). Within the same docking protocol, the lower predicted energy for MMP-9 suggested a more favorable docking pose for diosmin than that observed for TNF. These values were used for target prioritization and were not interpreted as direct experimental measures of binding affinity.

To evaluate the stability of the prioritized diosmin-MMP-9 pose under simulated solvent conditions, a 100-ns all-atom molecular dynamics simulation was performed. Representative structures at 0, 50, and 100 ns showed that diosmin remained within the selected MMP-9 binding pocket throughout the trajectory (Figure 6L). RMSD trajectories reached relatively stable plateaus after approximately 60 ns for the protein backbone and 40 ns for the ligand (Figure 6A-D). The Rg remained within approximately 1.77-1.83 nm (Figure 6H-I), and hydrogen-bond analysis showed recurrent interactions between diosmin and MMP-9 during the simulation (Figure 6G). RMSF analysis indicated lower fluctuations for several residues near the selected binding pocket than for more flexible loop regions (Figure 6E), while SASA fluctuated within approximately 115-131 nm^2 (Figure 6F).

MM-PBSA analysis yielded a favorable estimated interaction energy for the simulated diosmin-MMP-9 complex. Van der Waals and electrostatic terms contributed favorably, whereas polar-solvation energy opposed complex formation. Residue-wise decomposition identified TYR179, GLY178, ARG106, GLN108, VAL101, ASP177, PHE107, PHE192, PRO102, and PRO193 among residues with notable energetic contributions, with TYR179 showing the largest favorable contribution in this analysis (Figure 6J-K). Collectively, these simulations support the structural plausibility and dynamic persistence of the selected docking pose, but they do not by themselves demonstrate direct target engagement in cells.

3.5 CCK-8 assay for selection of experimental concentrations

CCK-8 dose-response experiments were conducted to identify a diosmin concentration without an obvious reduction in cell viability and an LPS

concentration producing a measurable but non-lethal injury phenotype (Figure 7). Diosmin at 0-80 μM did not significantly reduce SV-HUC-1 viability, whereas 90 μM significantly decreased viability (***P < 0.001 vs control). LPS at 1 μg/mL produced a moderate reduction in viability, while 2 μg/mL caused more pronounced cell loss. Accordingly, 80 μM diosmin with 1 μg/mL LPS was selected for subsequent experiments, with diosmin administered 1 h before LPS exposure.

3.6 Colony-formation assay evaluates proliferative recovery

Compared with the control group, LPS exposure reduced colony number and total colony area , consistent with impaired long-term proliferative capacity (Figure 8). Diosmin pretreatment significantly improved both colony number and colony area relative to the LPS group. These findings indicate that diosmin partially preserved or restored colony-forming capacity under the selected inflammatory-injury conditions.

3.7 NO quantification

LPS stimulation markedly increased NO-related products in the culture supernatant (****$P < 0.0001$ vs control; Figure 9). Diosmin pretreatment significantly reduced this LPS-associated increase ($P < 0.01$ vs LPS group). Thus, under the present experimental conditions, diosmin attenuated an LPS-induced increase in a nitrosative/inflammatory readout.

3.8 Western blot validation of candidate hub proteins

Western blotting was used to examine MMP-9,TNF-α and IL-17 three proteins (Figure 10). Relative to control cells, LPS exposure increased MMP-9, TNF-α andIL-17 protein abundance (*P < 0.05). Diosmin pretreatment reduced the LPS-associated increases in both proteins (#P < 0.05 vs LPS group). These results are consistent with an association between diosmin treatment and suppression of MMP-9/TNF-α/IL-17-related inflammatory responses.

4. Discussion

The present study combined network pharmacology, structural simulation, and cellular validation to investigate diosmin in an acute-cystitis-related urothelial inflammatory-injury model. UPEC infection of the bladder is shaped by dynamic interactions between bacterial virulence programs and urothelial innate responses [1, 2, 6-10, 44]. Excessive or poorly resolved host inflammation can contribute to epithelial dysfunction even while immune responses are required for bacterial control. In this context, our results show that diosmin attenuated several LPS-associated injury readouts in SV-HUC-1 cells, including impaired colony formation, increased NO-related products, and elevated MMP-9,TNF-α and IL-17 protein expression. These cellular findings complement, but should be distinguished from, the computational predictions.

Diosmin has previously been characterized as a pleiotropic flavonoid with anti-inflammatory and antioxidant effects in diverse experimental systems[11-19]. In particular, reductions in pro-inflammatory mediators and NF-κB/MAPK-related responses have been reported in LPS-stimulated macrophages, while TNF-α-related effects have also been observed in other cellular injury models [15, 16]. Our data extend this literature to SV-HUC-1 urothelial cells by showing that diosmin reduced LPS-associated TNF-α expression and NO accumulation and improved colony-forming capacity. Nevertheless, because LPS stimulation represents only one component of Gram-negative bacterial sensing, these observations should not be equated with demonstrated efficacy against live UPEC infection.

Network analysis prioritized MMP-9 and TNF as central nodes among the 11 overlapping targets. MMPs can remodel extracellular matrix and modulate inflammatory signaling, and MMP-9 (gelatinase B) is particularly well characterized as a regulator of matrix turnover and inflammatory processes [45-47]. TNF-α is a major cytokine with context-dependent effects on inflammatory cell activation, cell survival, and tissue injury [48]. IL-17 signaling, which emerged from KEGG enrichment in the present study, is also a key inflammatory pathway with extensive interactions with other cytokine networks [49-51]. Importantly, enrichment of TNF and IL-17 pathways does not establish a linear MMP-9→TNF-α→IL-17 cascade. The present data support co-involvement of these inflammatory modules, whereas their causal ordering requires targeted perturbation experiments.

Molecular docking and molecular dynamics simulation further prioritized MMP-9 as a plausible structural candidate. Diosmin showed a lower docking energy for MMP-9 than for TNF within the same docking workflow, and the selected diosmin-MMP-9 pose remained dynamically stable during the 100-ns simulation. MM-PBSA and residue-decomposition analyses provided additional computational support for the selected pose. However, docking scores and molecular dynamics trajectories are hypothesis-generating rather than direct measurements of cellular target engagement. The reduction in MMP-9 protein abundance observed after diosmin treatment is therefore compatible with, but does not prove, direct binding of diosmin to MMP-9. Biophysical target-engagement assays and genetic rescue experiments are required to distinguish direct binding from indirect transcriptional or post-transcriptional regulation.LPS reduced colony formation in SV-HUC-1 cells, whereas diosmin partially restored this phenotype. This result is consistent with preservation of epithelial proliferative capacity, but it does not directly measure urothelial barrier function. Future studies should incorporate transepithelial electrical resistance, permeability assays, junctional proteins, wound-healing assays, and differentiated urothelial models to more directly examine barrier integrity and repair.

NF-κB is a central transcriptional regulator that links innate immune stimulation to the expression of numerous inflammatory mediators [52], and prior diosmin studies have implicated NF-κB/MAPK modulation in its anti-inflammatory actions [15, 19]. NO and reactive nitrogen species can participate in host

defense but may also contribute to cellular injury when produced in excess [53-55]. In our model, LPS increased NO-related products, and diosmin significantly attenuated this response. The finding is biologically compatible with the broader ability of flavonoids to modulate inflammatory and redox-sensitive signaling[56, 57]. Because phosphorylation or nuclear translocation of NF-κB/MAPK components was not measured here, these pathways remain plausible upstream mechanisms rather than experimentally verified intermediates in the present study.Taken together, the computational and experimental data support a conservative working model in which diosmin reduces LPS-induced urothelial inflammatory injury and is associated with lower MMP-9,TNF-α and IL-17 expression.

Several limitations should be considered. First, all functional experiments were performed in an SV-HUC-1 monoculture model. This system does not reproduce the full bladder microenvironment, including immune-cell recruitment, stromal interactions, urine exposure, and mechanical factors. Second, LPS stimulation cannot recapitulate key features of live UPEC infection such as bacterial adhesion, invasion, intracellular community formation, persistence, and recurrent infection [6-10, 44]. Infection-based animal models and, ideally, organoid or differentiated urothelial systems are therefore needed. Third, target engagement was inferred from docking, molecular dynamics, and protein-expression changes rather than measured directly. MMP-9 knockdown/overexpression and pharmacological rescue experiments, together with orthogonal binding assays, would be necessary to establish whether MMP-9 is required for diosmin's protective phenotype. Finally, the small number of overlapping targets and the dependence of network pharmacology on database coverage mean that the computational results should be viewed as prioritization rather than exhaustive target identification.

Despite these limitations, the study has two strengths. First, it links database-derived target prioritization to a structurally evaluated candidate interaction and then to functional and molecular readouts in human urothelial cells. Second, the interpretation distinguishes computational association from experimental causality, thereby defining a clear path for follow-up work. Future studies should test diosmin in live-UPEC cystitis models, quantify bladder bacterial burden and histopathology, assess urothelial barrier function, and perform MMP-9-centered loss- and gain-of-function experiments. Such studies will be necessary before considering diosmin as a candidate adjunct for clinical acute cystitis.

5. Conclusions

In summary, diosmin attenuated LPS-induced inflammatory injury in SV-HUC-1 human urothelial cells, improved colony-forming capacity, reduced NO-related products, and decreased MMP-9 and TNF-α protein expression. Network pharmacology and structural simulations prioritized MMP-9 and TNF-IL-17-related pathways as candidate mechanistic components.These findings provide preliminary mechanistic evidence for further investigation of diosmin in acute-cystitis-related inflammatory injury. Infection-based in vivo studies, direct target-engagement assays, and genetic rescue experiments are

required before efficacy or a definitive molecular mechanism can be established.

References

1. Flores-Mireles, A.L., et al., *Urinary tract infections: epidemiology, mechanisms of infection and treatment options.* Nat Rev Microbiol, 2015. **13**(5): p. 269-84.
2. Klein, R.D. and S.J. Hultgren, *Urinary tract infections: microbial pathogenesis, host-pathogen interactions and new treatment strategies.* Nat Rev Microbiol, 2020. **18**(4): p. 211-226.
3. Bono, M.J. and S.W. Leslie, *Uncomplicated Urinary Tract Infections*, in *StatPearls*. 2026, StatPearls Publishing Copyright © 2026, StatPearls Publishing LLC.: Treasure Island (FL).
4. Gupta, K., et al., *International clinical practice guidelines for the treatment of acute uncomplicated cystitis and pyelonephritis in women: A 2010 update by the Infectious Diseases Society of America and the European Society for Microbiology and Infectious Diseases.* Clin Infect Dis, 2011. **52**(5): p. e103-20.
5. Ranjbar, R. and M. Alam, *Antimicrobial Resistance Collaborators (2022). Global burden of bacterial antimicrobial resistance in 2019: a systematic analysis.* Evid Based Nurs, 2023.
6. Anderson, G.G., et al., *Intracellular bacterial biofilm-like pods in urinary tract infections.* Science, 2003. **301**(5629): p. 105-7.
7. Hannan, T.J., et al., *Early severe inflammatory responses to uropathogenic E. coli predispose to chronic and recurrent urinary tract infection.* PLoS Pathog, 2010. **6**(8): p. e1001042.
8. Mysorekar, I.U. and S.J. Hultgren, *Mechanisms of uropathogenic Escherichia coli persistence and eradication from the urinary tract.* Proc Natl Acad Sci U S A, 2006. **103**(38): p. 14170-5.
9. Khandelwal, P., S.N. Abraham, and G. Apodaca, *Cell biology and physiology of the uroepithelium.* Am J Physiol Renal Physiol, 2009. **297**(6): p. F1477-501.
10. Song, J., et al., *TLR4-mediated expulsion of bacteria from infected bladder epithelial cells.* Proc Natl Acad Sci U S A, 2009. **106**(35): p. 14966-71.
11. Benavente-García, O. and J. Castillo, *Update on uses and properties of citrus flavonoids: new findings in anticancer, cardiovascular, and anti-inflammatory activity.* J Agric Food Chem, 2008. **56**(15): p. 6185-205.
12. Zheng, Y., et al., *Metabolism and pharmacological activities of the natural health-benefiting compound diosmin.* Food Funct, 2020. **11**(10): p. 8472-8492.
13. Gerges, S.H., et al., *Pharmacology of Diosmin, a Citrus Flavone Glycoside: An Updated Review.* Eur J Drug Metab Pharmacokinet, 2022. **47**(1): p. 1-18.
14. Crespo, M.E., et al., *Anti-inflammatory activity of diosmin and hesperidin in rat colitis induced by TNBS.* Planta Med, 1999. **65**(7): p. 651-3.
15. Berkoz, M., *Diosmin suppresses the proinflammatory mediators in lipopolysaccharide-induced RAW264.7 macrophages via NF-κB and MAPKs signal pathways.* Gen Physiol Biophys, 2019. **38**(4): p. 315-324.
16. Dholakiya, S.L. and K.E. Benzeroual, *Protective effect of diosmin on LPS-induced apoptosis in PC12 cells and inhibition of TNF-α expression.* Toxicol In Vitro, 2011. **25**(5): p. 1039-44.

17. Chen, Y.R., et al., *The chondroprotective effect of diosmin on human articular chondrocytes under oxidative stress.* Phytother Res, 2019. **33**(9): p. 2378-2386.
18. Feldo, M., et al., *Modulatory Effect of Diosmin and Diosmetin on Metalloproteinase Activity and Inflammatory Mediators in Human Skin Fibroblasts Treated with Lipopolysaccharide.* Molecules, 2022. **27**(13).
19. Zhao, W.M., et al., *Diosmin ameliorates renal fibrosis through inhibition of inflammation by regulating SIRT3-mediated NF-κB p65 nuclear translocation.* BMC Complement Med Ther, 2024. **24**(1): p. 29.
20. Hopkins, A.L., *Network pharmacology: the next paradigm in drug discovery.* Nat Chem Biol, 2008. **4**(11): p. 682-90.
21. Daina, A., O. Michielin, and V. Zoete, *SwissTargetPrediction: updated data and new features for efficient prediction of protein targets of small molecules.* Nucleic Acids Res, 2019. **47**(W1): p. W357-w364.
22. Keiser, M.J., et al., *Relating protein pharmacology by ligand chemistry.* Nat Biotechnol, 2007. **25**(2): p. 197-206.
23. Stelzer, G., et al., *The GeneCards Suite: From Gene Data Mining to Disease Genome Sequence Analyses.* Curr Protoc Bioinformatics, 2016. **54**: p. 1.30.1-1.30.33.
24. Wang, J.H., et al., *GenCLiP 2.0: a web server for functional clustering of genes and construction of molecular networks based on free terms.* Bioinformatics, 2014. **30**(17): p. 2534-6.
25. Amberger, J.S., et al., *OMIM.org: Online Mendelian Inheritance in Man (OMIM®), an online catalog of human genes and genetic disorders.* Nucleic Acids Res, 2015. **43**(Database issue): p. D789-98.
26. Barrett, T., et al., *NCBI GEO: archive for functional genomics data sets--update.* Nucleic Acids Res, 2013. **41**(Database issue): p. D991-5.
27. Szklarczyk, D., et al., *The STRING database in 2021: customizable protein-protein networks, and functional characterization of user-uploaded gene/measurement sets.* Nucleic Acids Res, 2021. **49**(D1): p. D605-d612.
28. Shannon, P., et al., *Cytoscape: a software environment for integrated models of biomolecular interaction networks.* Genome Res, 2003. **13**(11): p. 2498-504.
29. Yu, G., et al., *clusterProfiler: an R package for comparing biological themes among gene clusters.* Omics, 2012. **16**(5): p. 284-7.
30. Wu, T., et al., *clusterProfiler 4.0: A universal enrichment tool for interpreting omics data.* Innovation (Camb), 2021. **2**(3): p. 100141.
31. Ashburner, M., et al., *Gene ontology: tool for the unification of biology. The Gene Ontology Consortium.* Nat Genet, 2000. **25**(1): p. 25-9.
32. Kanehisa, M. and S. Goto, *KEGG: kyoto encyclopedia of genes and genomes.* Nucleic Acids Res, 2000. **28**(1): p. 27-30.
33. Burley, S.K., et al., *RCSB Protein Data Bank: biological macromolecular structures enabling research and education in fundamental biology, biomedicine, biotechnology and energy.* Nucleic Acids Res, 2019. **47**(D1): p. D464-d474.
34. Kim, S., et al., *PubChem 2023 update.* Nucleic Acids Res, 2023. **51**(D1): p. D1373-d1380.
35. Trott, O. and A.J. Olson, *AutoDock Vina: improving the speed and accuracy of docking with a new scoring function, efficient optimization, and multithreading.* J Comput Chem, 2010. **31**(2): p. 455-61.
36. Antalík, A., et al., *MiMiC: A high-performance framework for multiscale molecular dynamics simulations.* J Chem Phys, 2024. **161**(2).

37. Huang, J. and A.D. MacKerell, Jr., *CHARMM36 all-atom additive protein force field: validation based on comparison to NMR data.* J Comput Chem, 2013. **34**(25): p. 2135-45.
38. Paesani, F., et al., *An accurate and simple quantum model for liquid water.* J Chem Phys, 2006. **125**(18): p. 184507.
39. Kumari, R., R. Kumar, and A. Lynn, *g_mmpbsa--a GROMACS tool for high-throughput MM-PBSA calculations.* J Chem Inf Model, 2014. **54**(7): p. 1951-62.
40. Tsukatani, T., et al., *Rapid susceptibility testing for slowly growing nontuberculous mycobacteria using a colorimetric microbial viability assay based on the reduction of water-soluble tetrazolium WST-1.* Eur J Clin Microbiol Infect Dis, 2015. **34**(10): p. 1965-73.
41. Alberts, D.S., et al., *In-vitro clonogenic assay for predicting response of ovarian cancer to chemotherapy.* Lancet, 1980. **2**(8190): p. 340-2.
42. Tsikas, D., *Analysis of nitrite and nitrate in biological fluids by assays based on the Griess reaction: appraisal of the Griess reaction in the L-arginine/nitric oxide area of research.* J Chromatogr B Analyt Technol Biomed Life Sci, 2007. **851**(1-2): p. 51-70.
43. *One-Way Analysis of Variance (ANOVA) – Including Dunnett's and Tukey's Follow Up Tests*, in *A Practical Approach to Using Statistics in Health Research*. 2018. p. 93-103.
44. Mulvey, M.A., et al., *Induction and evasion of host defenses by type 1-piliated uropathogenic Escherichia coli.* Science, 1998. **282**(5393): p. 1494-7.
45. Parks, W.C., C.L. Wilson, and Y.S. López-Boado, *Matrix metalloproteinases as modulators of inflammation and innate immunity.* Nat Rev Immunol, 2004. **4**(8): p. 617-29.
46. Vandooren, J., P.E. Van den Steen, and G. Opdenakker, *Biochemistry and molecular biology of gelatinase B or matrix metalloproteinase-9 (MMP-9): the next decade.* Crit Rev Biochem Mol Biol, 2013. **48**(3): p. 222-72.
47. Alamgeer, et al., *Phytochemicals targeting matrix metalloproteinases regulating tissue degradation in inflammation and rheumatoid arthritis.* Phytomedicine, 2020. **66**: p. 153134.
48. Kalliolias, G.D. and L.B. Ivashkiv, *TNF biology, pathogenic mechanisms and emerging therapeutic strategies.* Nat Rev Rheumatol, 2016. **12**(1): p. 49-62.
49. Amatya, N., A.V. Garg, and S.L. Gaffen, *IL-17 Signaling: The Yin and the Yang.* Trends Immunol, 2017. **38**(5): p. 310-322.
50. McGeachy, M.J., D.J. Cua, and S.L. Gaffen, *The IL-17 Family of Cytokines in Health and Disease.* Immunity, 2019. **50**(4): p. 892-906.
51. Souto-Silva, M.V., et al., *The cytokine-skin barrier axis in health and disease.* Cytokine Growth Factor Rev, 2026. **87**: p. 113-123.
52. Sun, S.C., *The non-canonical NF-κB pathway in immunity and inflammation.* Nat Rev Immunol, 2017. **17**(9): p. 545-558.
53. Pacher, P., J.S. Beckman, and L. Liaudet, *Nitric oxide and peroxynitrite in health and disease.* Physiol Rev, 2007. **87**(1): p. 315-424.
54. Förstermann, U. and W.C. Sessa, *Nitric oxide synthases: regulation and function.* Eur Heart J, 2012. **33**(7): p. 829-37, 837a-837d.
55. Radi, R., *Peroxynitrite, a stealthy biological oxidant.* J Biol Chem, 2013. **288**(37): p. 26464-72.
56. Zaragozá, C., et al., *Potential Therapeutic Anti-Inflammatory and Immunomodulatory Effects of Dihydroflavones, Flavones, and Flavonols.* Molecules, 2020. **25**(4).
57. Pan, M.H., C.S. Lai, and C.T. Ho, *Anti-inflammatory activity of natural dietary flavonoids.* Food Funct, 2010. **1**(1): p. 15-31.

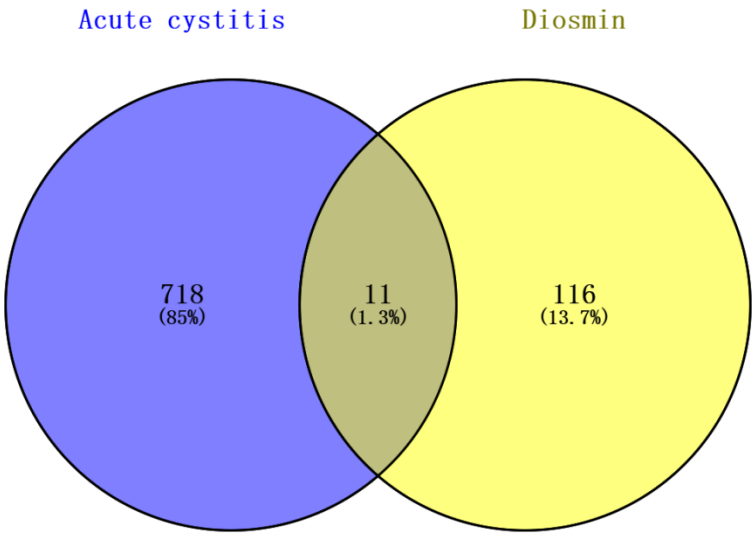


Figure 1. Venn diagram of overlapping targets between diosmin-predicted targets and acute-cystitis-related genes. Candidate therapeutic targets of diosmin were predicted from Swiss-TargetPrediction and SEA databases. Acute-cystitis-associated genes were collected from GEO datasets (GSE33210, GSE26509), Gene Cards, Geneclips and OMIM databases. After deduplication, 11 intersecting target genes were obtained.

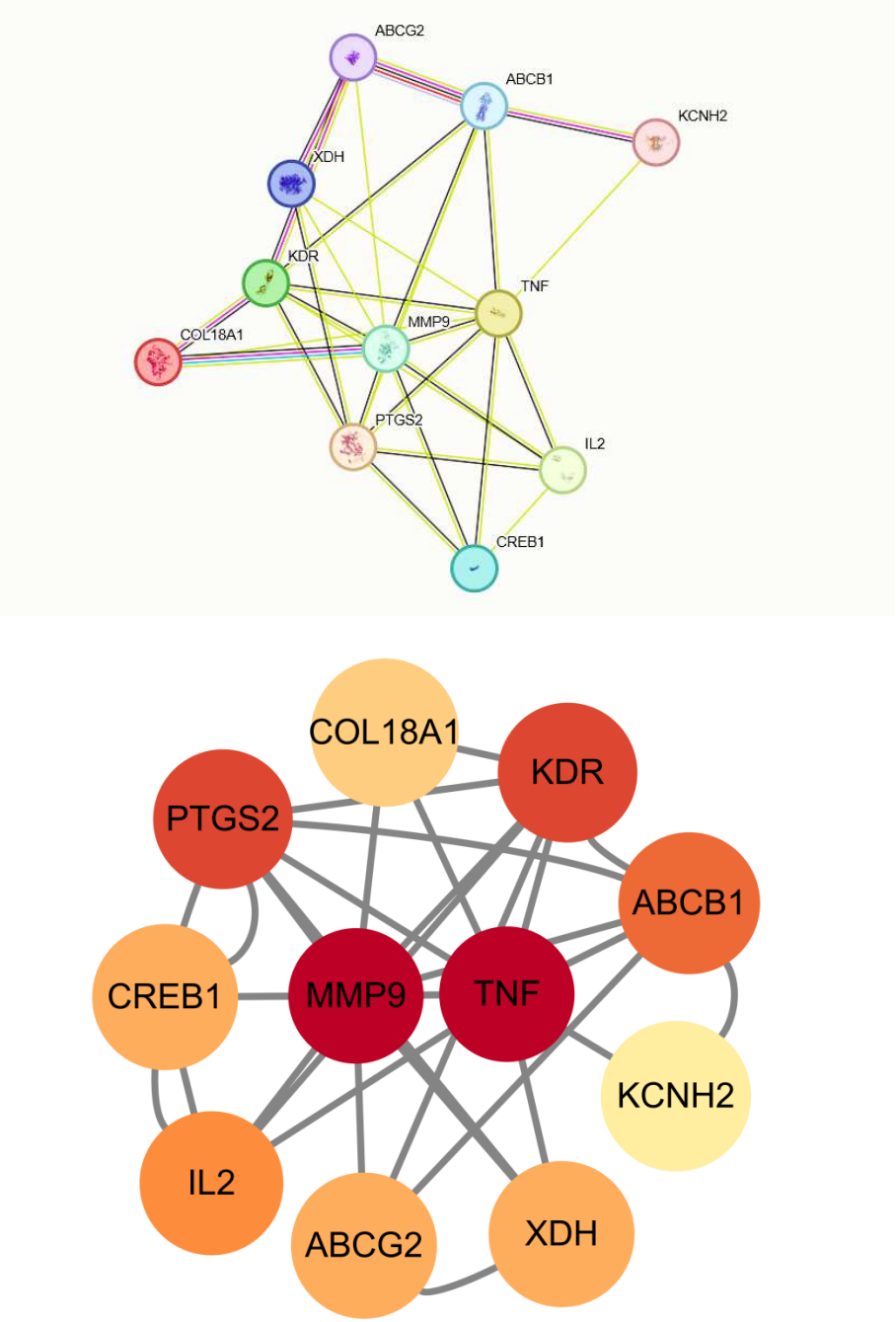


Figure 2. PPI network and hub-gene screening of intersection targets. Eleven overlapping target genes were imported into STRING database (confidence score >0.7). Interaction data were imported into Cytoscape 3.9.1 software for topological-degree-value calculation. TNF and MMP-9 were identified as top-two hub genes.

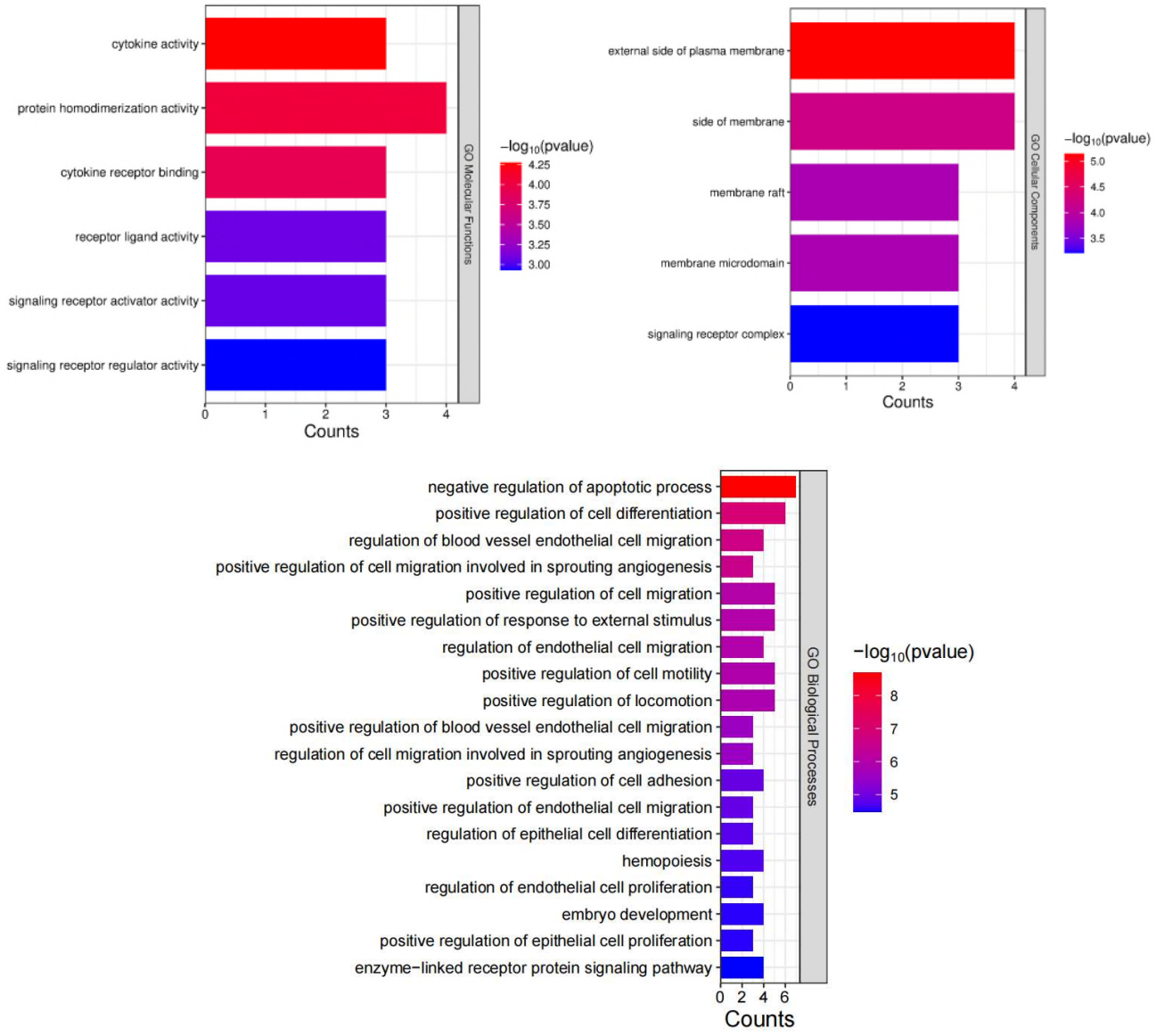


Figure 3. Gene Ontology (GO) enrichment analysis of overlapping target genes.GO enrichment analysis covered biological process (BP), cellular component (CC) and molecular function (MF). The bar graph displays significantly enriched GO terms ($P < 0.05$), reflecting potential biological functions modulated by diosmin against acute cystitis.

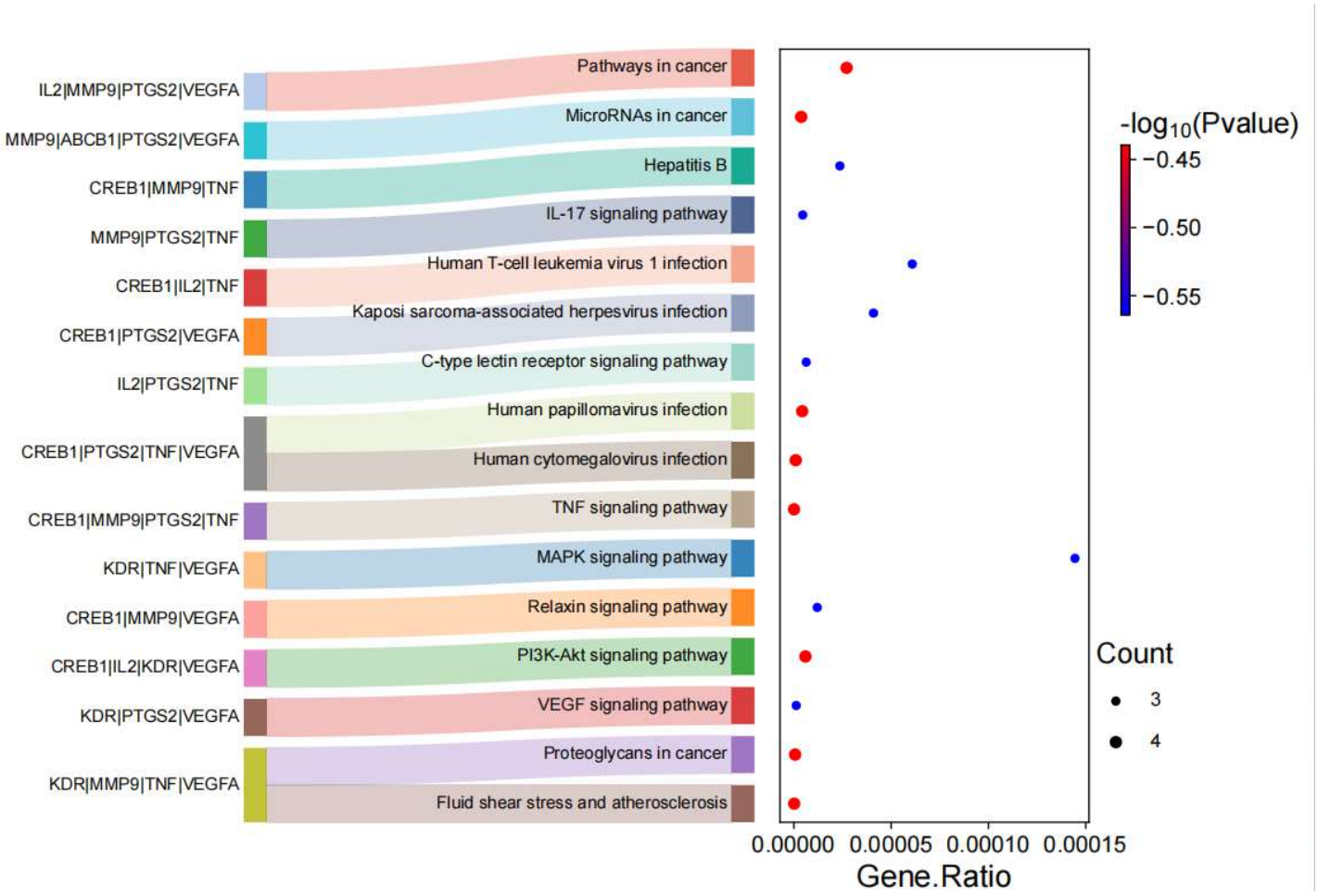


Figure 4. Kyoto Encyclopedia of Genes and Genomes (KEGG) pathway enrichment analysis. Bubble diagram shows significantly enriched KEGG pathways ($P < 0.05$). The TNF and IL-17 signaling pathways were prominently enriched, indicating the potential inflammatory-regulatory mechanism of diosmin.

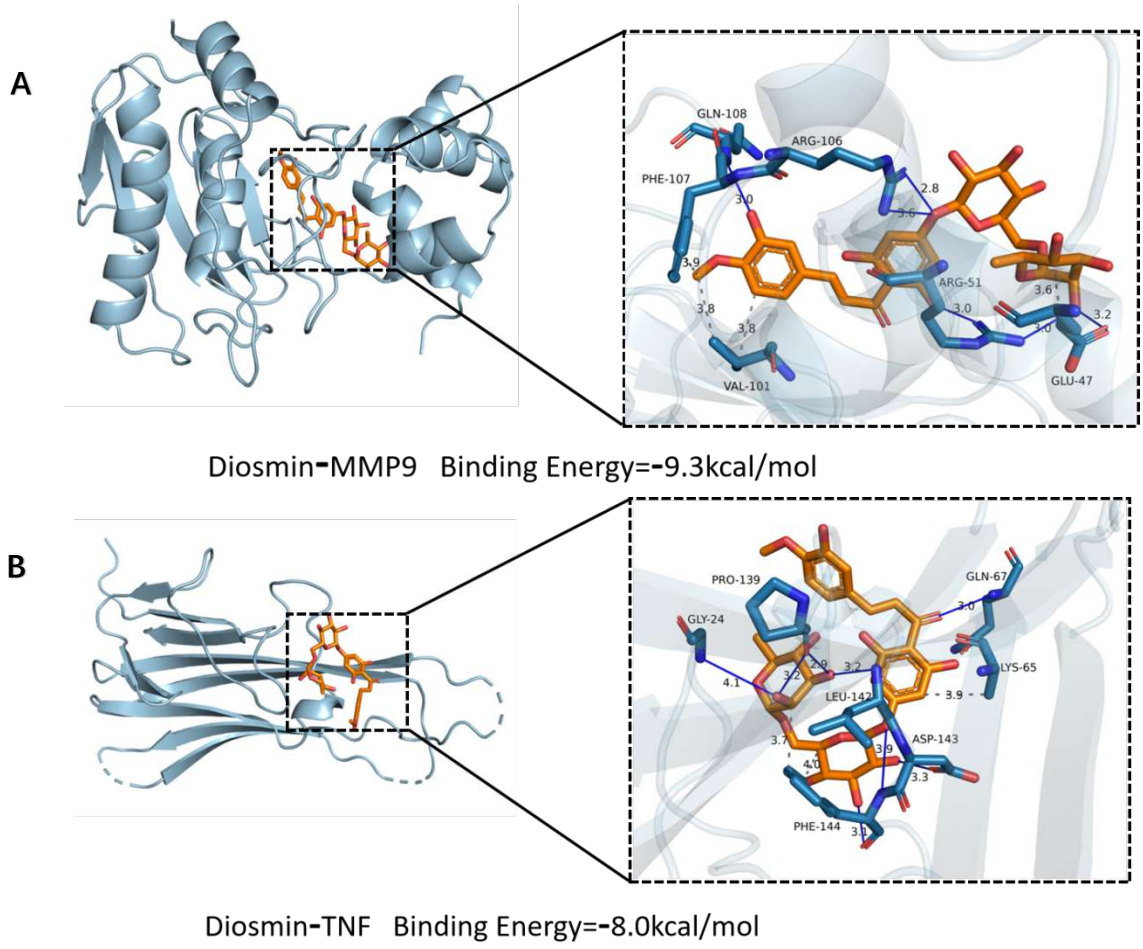


Figure 5. Molecular docking results of TNF,MMP9 and Diosmin.(A)Docking conformation of diosmin-MMP-9 complex, binding energy = −9.3 kcal/mol. (B) Docking conformation of diosmin-TNF complex, binding energy = −8.0 kcal/mol.

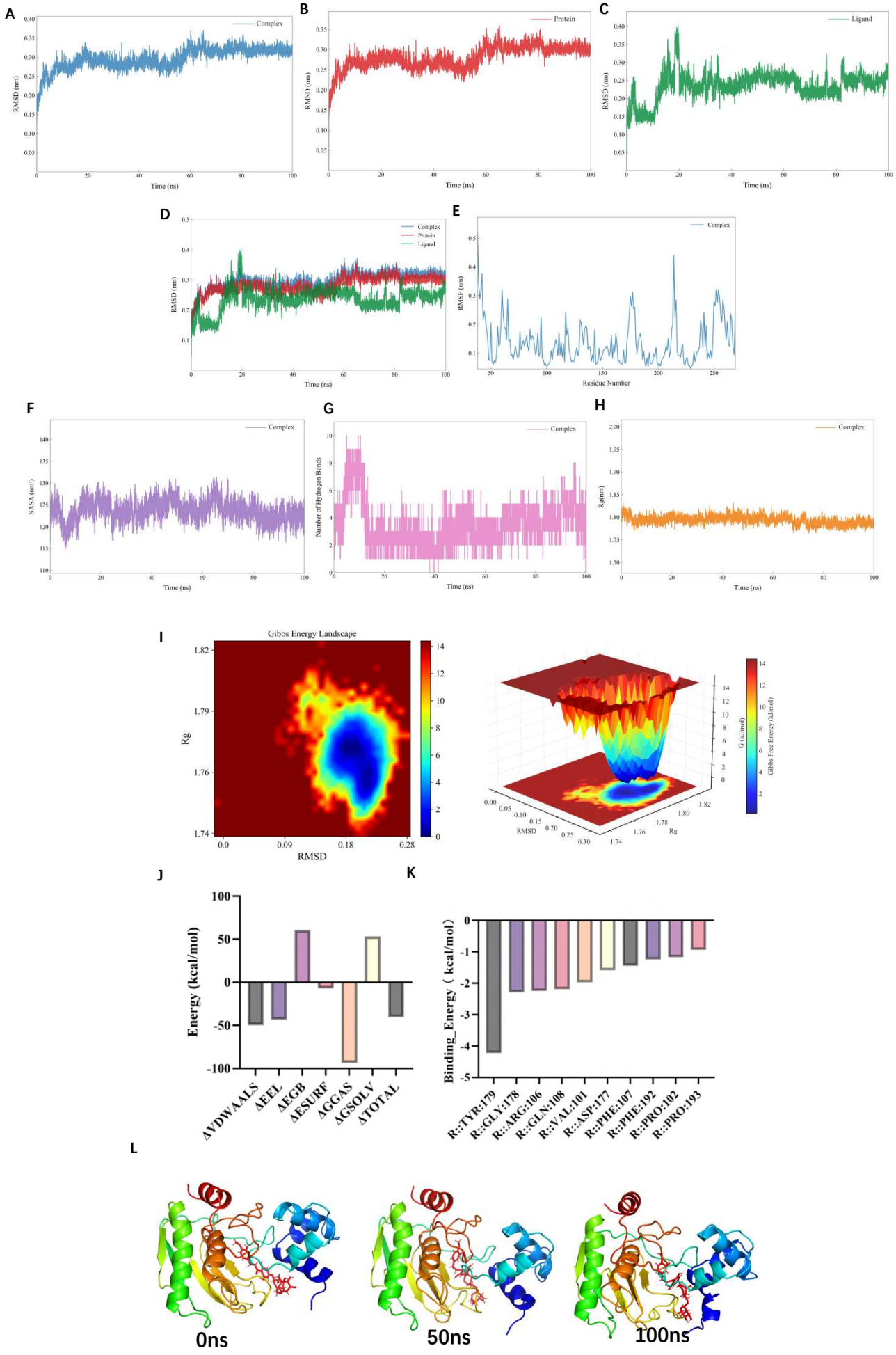

A
Complex
RMSD (nm)
Time (ns)
B
Protein
RMSD (nm)
Time (ns)
C
Ligand
RMSD (nm)
Time (ns)
D
Complex
Protein
Ligand
RMSD (nm)
Time (ns)
E
Complex
RMSF (nm)
Residue Number
F
Complex
SASA (nm²)
Time (ns)
G
Complex
Number of Hydrogen Bonds
Time (ns)
H
Complex
Rg(nm)
Time (ns)
I
Gibbs Energy Landscape
Rg
RMSD
G (kJ/mol)
Gibbs Free Energy (kJ/mol)
J
Energy (kcal/mol)
ΔVDWAALS
ΔEEL
ΔEGB
ΔESURF
ΔGGAS
ΔGSOLV
ΔTOTAL
K
Binding_Energy（kcal/mol)
R::TYR:179
R::GLY:178
R::ARG:106
R::GLN:108
R::VAL:101
R::ASP:177
R::PHE:107
R::PHE:192
R::PRO:102
R::PRO:193
L
0ns
50ns
100ns

Figure 6. Trajectory analysis of 100 ns molecular dynamics simulation for the diosmin-MMP-9 complex.(A-D) RMSD curves of MMP-9 backbone and diosmin ligand;(E) RMSF profile of MMP-9 residues; (F) SASA curve of the diosmin-MMP-9 complex;(G) Time-dependent hydrogen-bond number between diosmin and MMP-9; (H-I) Radius of gyration (Rg) of the complex; (J-K) Residue-based energy decomposition from MM-PBSA calculation; (L)Representative 3D conformations of diosmin-MMP-9 complex captured at 0 ns, 50 ns and 100 ns.Simulation results demonstrated stable structural and thermodynamic binding between diosmin and MMP-9.

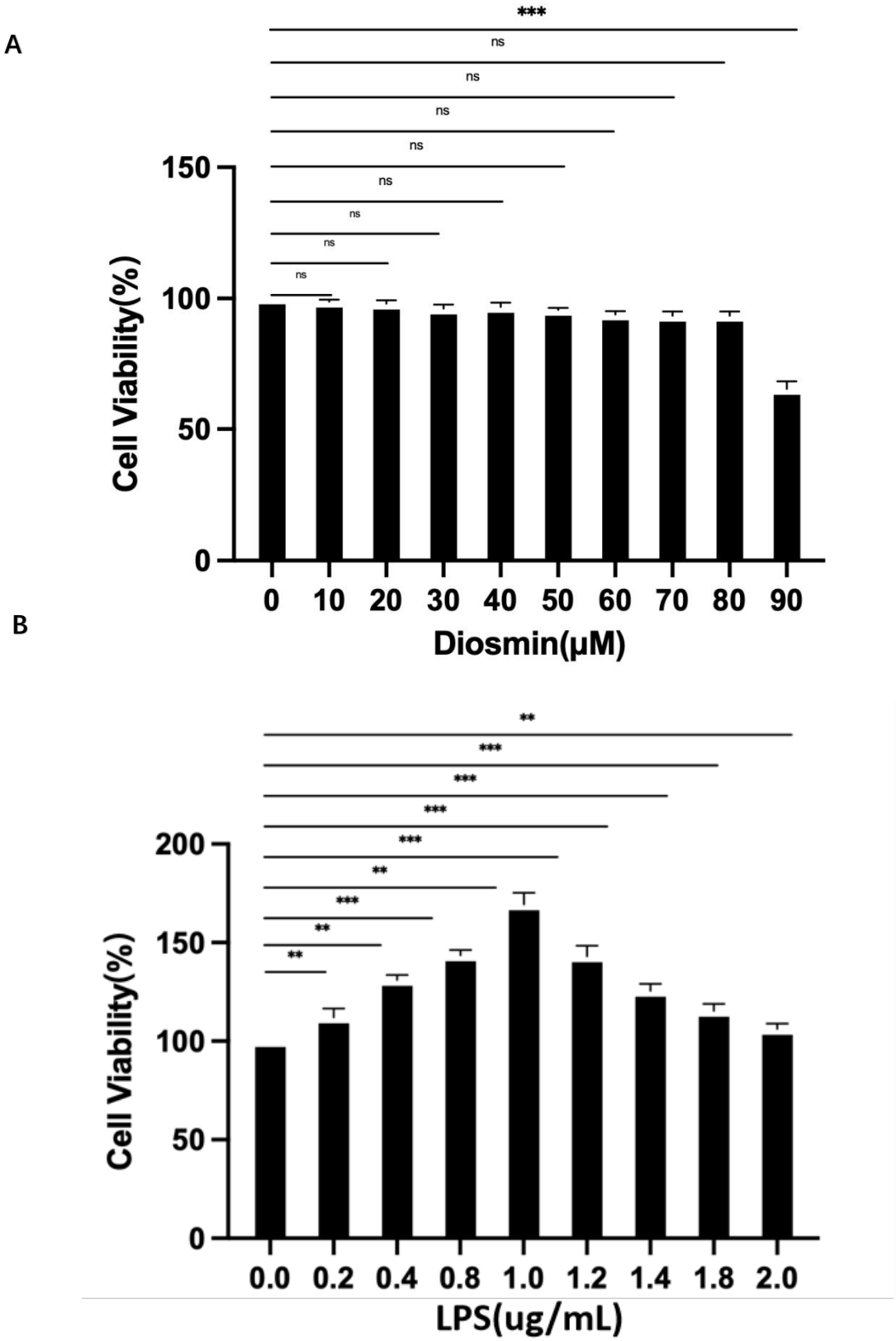


Figure 7. CCK-8 cell-viability assay for concentration-gradient screening. (A) Cell viability of SV-HUC-1 cells treated with gradient diosmin concentrations (0-90 μM). (B) Cell viability under gradient LPS stimulation (0-2 μg/mL). Data are presented as mean ± SD (n = 3). ns: not-significant; ***P<0.001 vs control group. One-way ANOVA followed by Tukey's post-hoc test.

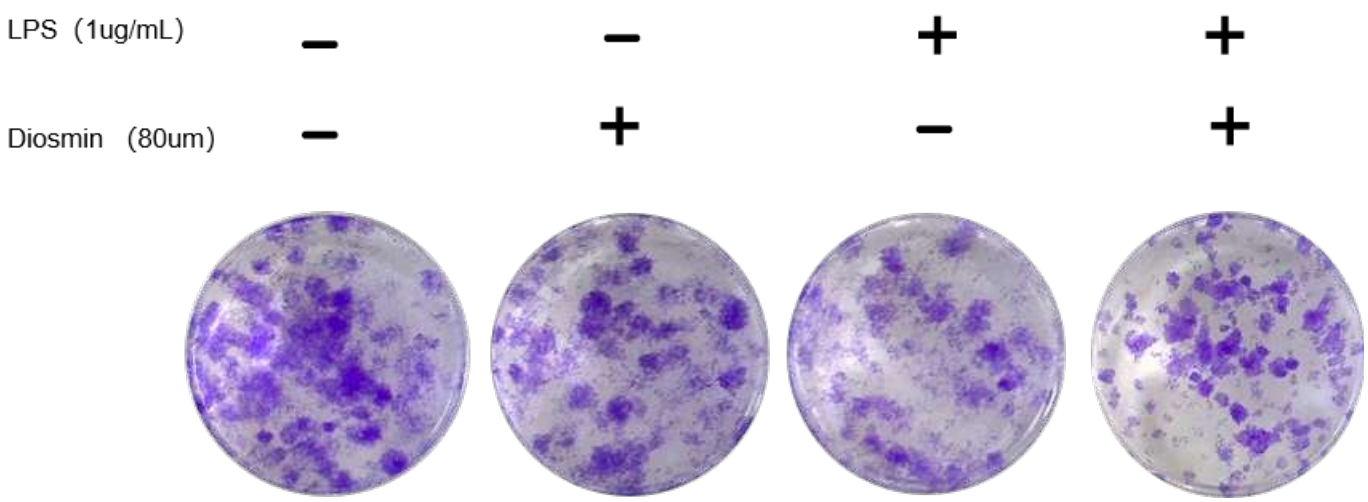


Figure 8. Clone-formation assay assessing epithelial long-term proliferative-repair capacity. Representative crystal-violet-stained clone images and quantitative statistics of colony number and colony area. LPS significantly suppressed clone-forming capacity; diosmin pretreatment restored proliferative potential.

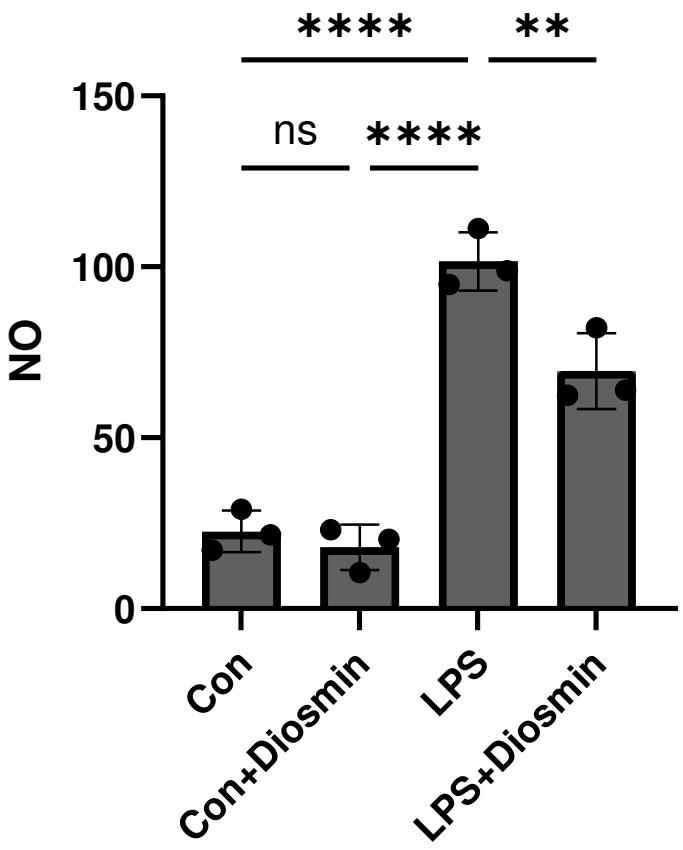


Figure 9. Quantitative detection of NO concentration in cell-culture supernatant. LPS induced significant NO over-production; diosmin intervention reduced NO release. Data are presented as mean ± SD (n = 3). ****P<0.0001 vs control group; **P<0.01 vs LPS group. One-way ANOVA followed by Tukey's post-hoc test.

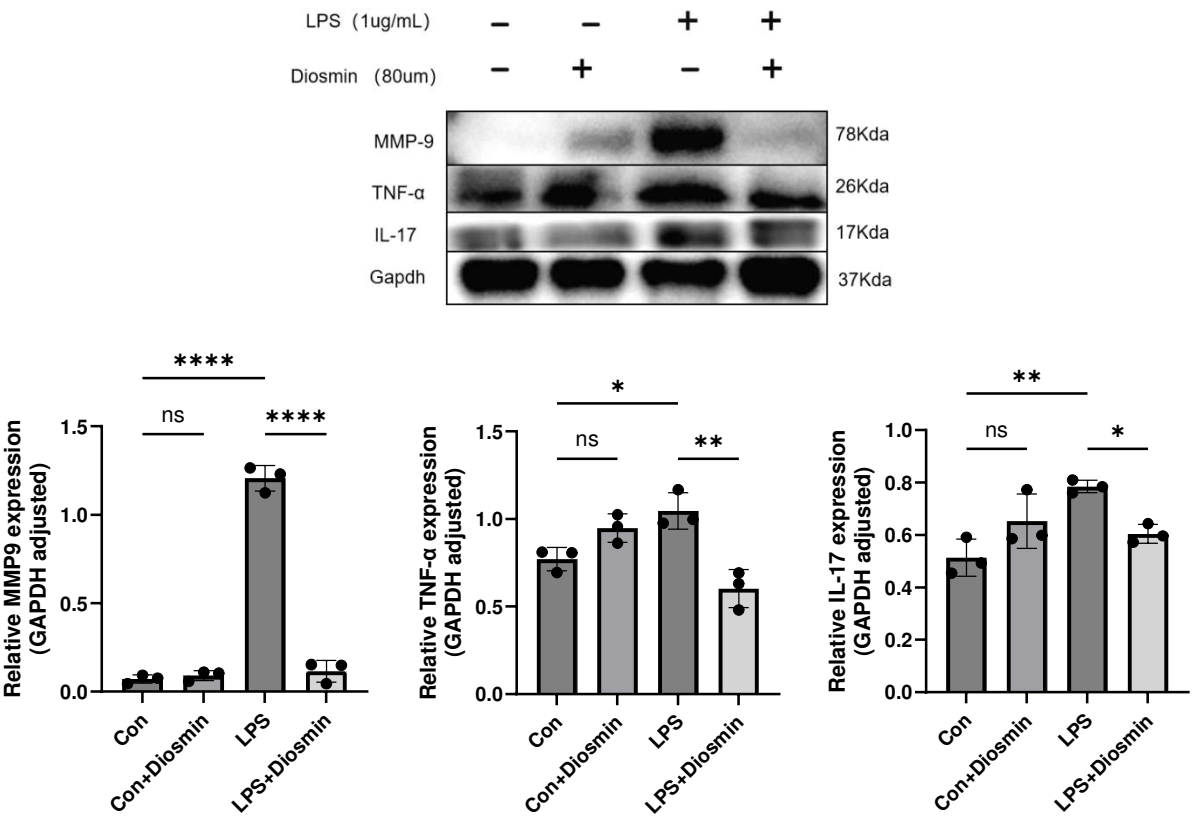


Figure 10. Western-blot bands of MMP-9、TNF-α and IL-17. Gapdh served as internal loading reference. LPS up-regulated MMP-9、TNF-α and IL-17; diosmin reversed this up-regulation.

Supplementary Files

This is a list of supplementary files associated with this preprint. Click to download.

- Tables.docx
- SupplementaryMaterials.docx